

University of Groningen

Axonal abnormalities in vanishing white matter

Klok, Melanie D.; Bugiani, Marianna; de Vries, Sharon I.; Gerritsen, Wouter; Breur, Marjolein; van der Sluis, Sophie; Heine, Vivi M.; Kole, Maarten H. P.; Baron, Wietske; van der Knaap, Marjo S.

Published in:
Annals of Clinical and Translational Neurology

DOI:
[10.1002/acn3.540](https://doi.org/10.1002/acn3.540)

IMPORTANT NOTE: You are advised to consult the publisher's version (publisher's PDF) if you wish to cite from it. Please check the document version below.

Document Version
Publisher's PDF, also known as Version of record

Publication date:
2018

[Link to publication in University of Groningen/UMCG research database](#)

Citation for published version (APA):

Klok, M. D., Bugiani, M., de Vries, S. I., Gerritsen, W., Breur, M., van der Sluis, S., ... van der Knaap, M. S. (2018). Axonal abnormalities in vanishing white matter. *Annals of Clinical and Translational Neurology*, 5(4), 429-444. DOI: 10.1002/acn3.540

Copyright

Other than for strictly personal use, it is not permitted to download or to forward/distribute the text or part of it without the consent of the author(s) and/or copyright holder(s), unless the work is under an open content license (like Creative Commons).


Take-down policy

If you believe that this document breaches copyright please contact us providing details, and we will remove access to the work immediately and investigate your claim.

Downloaded from the University of Groningen/UMCG research database (Pure): <http://www.rug.nl/research/portal>. For technical reasons the number of authors shown on this cover page is limited to 10 maximum.

RESEARCH ARTICLE

Axonal abnormalities in vanishing white matter

Melanie D. Klok¹, Marianna Bugiani², Sharon I. de Vries³, Wouter Gerritsen², Marjolein Breur², Sophie van der Sluis⁴, Vivi M. Heine^{1,4} , Maarten H. P. Kole^{3,5}, Wia Baron⁶ & Marjo S. van der Knaap^{1,7}

¹Department of Pediatrics/Child Neurology, Amsterdam Neuroscience, VU University Medical Centre, Amsterdam, The Netherlands

²Department of Pathology, Amsterdam Neuroscience, VU University Medical Centre, Amsterdam, The Netherlands

³Department of Axonal Signaling, Netherlands Institute for Neuroscience, Amsterdam, The Netherlands

⁴Department of Complex Trait Genetics, Center for Neurogenomics and Cognitive Research, Amsterdam Neuroscience, VU University Medical Centre, Amsterdam, The Netherlands

⁵Cell Biology, Faculty of Science, Utrecht University, Utrecht, The Netherlands

⁶Department of Cell Biology, University Medical Center Groningen, University of Groningen, Groningen, The Netherlands

⁷Department of Functional Genomics, Center for Neurogenomics and Cognitive Research, Amsterdam Neuroscience, VU University, Amsterdam, The Netherlands

Correspondence

Marjo S. van der Knaap, Department of Child Neurology, VU University Medical Centre, de Boelelaan 1117, 1081 HV Amsterdam, The Netherlands. Tel: +31 (0)20 4444856; Fax: 31 (0)20 444 0849; E-mail: ms.vanderknaap@vumc.nl

Funding Information

This work was supported by a grant from the Zeldzame Ziekten Fonds, The Netherlands. SvdS is funded by the Netherlands Scientific Organization (NWO/MaGW: VIDI-452-12-014). VMH is supported by ZonMw VIDI research grant 91712343 and E-Rare Joint Call project 9003037601. MSvdK is supported by the NWO Spinoza grant.

Received: 13 December 2017; Accepted: 30 December 2017

Annals of Clinical and Translational Neurology 2018; 5(4): 429–444

doi: 10.1002/acn3.540

Introduction

Vanishing white matter (VWM) commonly presents in early childhood, but onset may vary between antenatal period to senescence.¹ Age of onset is inversely related to clinical severity.² Clinically, VWM is characterized by chronic neurological decline with additional episodes of rapid, severe deterioration provoked by stressors like

febrile infections and minor head trauma, which may end in coma and death.^{3–6} As yet, no curative treatment is available.

VWM is caused by mutations in the genes encoding the five subunits of the eukaryotic translation initiation factor 2B (eIF2B), *EIF2B1* through *EIF2B5*.^{7,8} eIF2B is an enzyme complex essential for translation of mRNAs into proteins and central in downregulating the rate of

Abstract

Objective: We aimed to study the occurrence and development of axonal pathology and the influence of astrocytes in vanishing white matter. **Methods:** Axons and myelin were analyzed using electron microscopy and immunohistochemistry on *Eif2b4* and *Eif2b5* single- and double-mutant mice and patient brain tissue. In addition, astrocyte-forebrain co-culture studies were performed. **Results:** In the corpus callosum of *Eif2b5*-mutant mice, myelin sheath thickness, axonal diameter, and G-ratio developed normally up to 4 months. At 7 months, however, axons had become thinner, while in control mice axonal diameters had increased further. Myelin sheath thickness remained close to normal, resulting in an abnormally low G-ratio in *Eif2b5*-mutant mice. In more severely affected *Eif2b4*-*Eif2b5* double-mutants, similar abnormalities were already present at 4 months, while in milder affected *Eif2b4* mutants, few abnormalities were observed at 7 months. Additionally, from 2 months onward an increased percentage of thin, unmyelinated axons and increased axonal density were present in *Eif2b5*-mutant mice. Co-cultures showed that *Eif2b5* mutant astrocytes induced increased axonal density, also in control forebrain tissue, and that control astrocytes induced normal axonal density, also in mutant forebrain tissue. In vanishing white matter patient brains, axons and myelin sheaths were thinner than normal in moderately and severely affected white matter. In mutant mice and patients, signs of axonal transport defects and cytoskeletal abnormalities were minimal. **Interpretation:** In vanishing white matter, axons are initially normal and atrophy later. Astrocytes are central in this process. If therapy becomes available, axonal pathology may be prevented with early intervention.

translation under different stress conditions.⁹ It is unclear why mutations in this housekeeping factor lead to a disorder specifically affecting the brain white matter, whereas other organs are mostly spared.¹⁰

The neuropathological findings in VWM include diffuse lack of myelin and cystic degeneration of the cerebral white matter.^{5,11} U-fibers, corpus callosum, internal capsule, and brainstem are better preserved.^{5,6,12} Considering the degree of cerebral white matter damage, reactive astrogliosis is disproportionately meager.^{13,14} Astrocytes are dysmorphic and immature.^{13–15} In relatively preserved white matter areas, lack of myelin is associated with increased numbers of oligodendrocyte progenitor cells (OPCs), while mature, myelinating oligodendrocytes are scarce.^{13,16,17}

Axons are lost in cavitated white matter and their numbers are variable in less severely involved areas.^{5,6,12,13,18} Remaining axons have been reported as abnormally thin.⁶ Axonal swellings and spheroids have been described around cavitated areas and in the subcortical white matter.^{19,20} Otherwise, axons have been reported as microscopically intact with a normal cytoskeleton at ultrastructural level.^{13,19,21} Cortex and central gray matter structures remain largely preserved without evident neuronal loss.^{5,6,13,14,18,20}

White matter astrocytes and oligodendrocytes are selectively affected.^{11,14,15,22} Recent studies indicate that astrocyte dysfunction is primary and oligodendrocyte dysfunction secondary.^{16,23} As astrocytes and oligodendrocytes are important for axonal support, their dysfunction in VWM may affect axonal integrity and function, but a primary axonal defect in VWM has not been ruled out.^{24–26} In this study, we investigated axonal morphology in brain tissue of VWM patients and mutant mice, in the latter at different time points, and used primary cell cultures to assess whether axonal abnormalities are primary or secondary to abnormality of VWM astrocytes.

Materials and Methods

Animals

Mouse models (background strain C57Bl/6J) were generated by inserting a point mutation in *Eif2b4* (*Eif2b4Arg484Trp/Arg484Trp*) or *Eif2b5* (*Eif2b5Arg191His/Arg191His*) and bred into homozygous single mutants as well as heterozygous-homozygous double-mutants, which in increasing order of severity are referred to as, respectively, *2b4^{ho}*, *2b5^{ho}*, and *2b4/2b5^{heho}* mice.²³ These mice replicate the human disease in clinical and pathological features and in variation in severity. Timed mating was performed with wild-type or mutant mice, with the day of plugging denoted as embryonic day 0 (E0).

Cell culture

Astrocytes or forebrain mixed cells were isolated from cerebral hemispheres of E18 mice and cultured following previously described methods with minor modifications.^{27–31} Cultures were kept in a humidified incubator at 37°C and 7.5% CO₂ at all times. For astrocyte cultures, cells were passaged two times, frozen and stored in liquid nitrogen until further use. Before starting a co-culture, astrocytes were first plated into a flask and cultured for 1 week in order to let them recover. Astrocyte-forebrain co-cultures were performed in poly-L-lysine-coated 96-well plates (Greiner). Fifteen thousand astrocytes were plated per well and cultured until confluence (4 days), after which 15,000 forebrain mixed cells, including neurons, oligodendrocytes, microglia, and a few astrocytes per well were plated on top of the astrocytes. Multiple wells with astrocytes were maintained without forebrain cells in order to determine astrocyte monolayer purity. As previously described, for the first 11 days, the co-culture medium contained insulin, followed by 17 days without insulin but with triiodothyronine (T3, Sigma-Aldrich). Half of the medium was replaced with fresh medium 3 times a week. Experiments were performed at least four independent times with at least three replicates per combination of astrocyte-forebrain co-culture.

Immunocytochemistry

Cells were fixed with 4% paraformaldehyde (PFA, Thermo Scientific) and 4% sucrose (Sigma-Aldrich) for 20 min at room temperature, washed two times with PBS, and permeabilized and blocked with 0.5% Triton X100 (Sigma-Aldrich) and 10% normal goat serum (Gibco) in PBS for 1 h at room temperature. Subsequently, cells were stained overnight at 4°C with primary antibodies in staining solution containing PBS, 0.1% Triton X100, and 10% normal goat serum. Then, cells were washed three times with PBS, followed by a 2-h incubation of secondary antibodies in staining solution. Finally, cells were washed two times with PBS and stored in PBS at 4°C until further analysis.

Primary antibodies used were directed against neuronal nuclei (NeuN, MAB377, 1:150, Millipore), microtubule-associated protein 2 (MAP2, AB5543, 1:3000, Chemicon), neurofilament 165 (NF165, 2H3, 1:250, Hybridoma Bank), neurofilament 200 (NF200, N4142, 1:2000, Sigma-Aldrich), phosphorylated neurofilament (SMI-31R, 1:1000, Covance), nonphosphorylated neurofilament (SMI-32R, 1:1000, Covance), vesicular glutamate transporter 1 (VGLUT1, AB5905, 1:5000, Millipore), postsynaptic density 95 (PSD95, MA1-046, 1:250, Thermo Scientific), myelin basic protein (MBP, ab7349, 1:400,

Abcam), oligodendrocyte nuclei (Olig2, AB9610, 1:1000, Chemicon), microglia (CD11b, M1/70.15.11.5.2, 1:50, Hybridoma Bank), chondroitin sulfate proteoglycan (NG2, AB5320, 1:200, Millipore), and glial fibrillary acidic protein (GFAP, ZO334, 1:1000, Dako). Secondary antibodies conjugated to Alexa Fluor (Thermo Fisher Scientific) 488, 568, 594 (all 1:1000) or 647 (1:800) were used as appropriate. Nuclei were stained with Hoechst (0.2 $\mu\text{g}/\text{mL}$, Molecular Probes).

Imaging

Culture plates were scanned using the Opera LX high content screening system (PerkinElmer). For each condition, three wells for astrocyte monolayers or five to six wells for astrocyte-forebrain co-cultures were analyzed. For cell counts, 14 images (20x objective) were captured per well. For quantitative analysis of neurite densities and MBP, 30 images (40x objective) were captured per well. For quantitative analysis of synapses 50 images (40x objective) were captured per well.

Quantitative analysis

Quantitative analysis was performed using Columbus 2.2 (PerkinElmer). Neurite (NF165, NF200, SMI31, or SMI32 for axons and MAP2 for dendrites) densities were given as area occupied by neurites relative to total area of the image (with or without correction for differences in number of NeuN⁺ neurons). MBP was quantified as area occupied by MBP immunoreactivity relative to total area of the image. Synaptic density was calculated by counting synapses (VGLUT1⁺ or PSD95⁺) located on top of a dendrite or within a distance of 1.6 μm from a dendrite and dividing the number by total dendrite length per image. Co-localization of VGLUT1⁺ and PSD95⁺ was determined by searching for PSD95⁺ spots located on top of VGLUT1⁺ spots or within a distance of 0.65 μm from VGLUT1⁺ spots. SMI31- or SMI32-positive neurites were quantified when co-localized with NF200- or MAP2-positive neurites and given as total length in μm per well or as total length ratio relative to NF200 or MAP2. Percentage of microglia present in the astrocyte monolayer was determined by counting CD11b-positive cells relative to the number of nuclei (oligodendrocytes or neurons were not detected).

Electron microscopy

Previously, we reported on electron microscopy (EM) analysis of corpus callosum of 7-month-old wild-type, *2b4^{ho}* and *2b5^{ho}* mice and 4-month-old *2b4/2b5^{heho}* mice, because the latter do not live up to 7 months.²³ Here, we additionally analyzed wild-type and *2b5^{ho}* mouse corpus

callosum at 2 and 4 months (two animals per group). Mouse brains were drop-fixed in 2% glutaraldehyde and 4% PFA in 0.1 mol/L sodium cacodylate buffer (pH 7.4). Human EM analysis included formalin-fixed corpus callosum tissue of a female 10-year-old control subject that died due to a brainstem tumor and a female 10-year-old patient diagnosed with classical VWM. Corpus callosum was dissected, postfixed in 1% osmium tetroxide and 1.5% potassium ferricyanide in 0.1 mol/L sodium cacodylate buffer, dehydrated and embedded in epoxy resin. Sagittally cut ultrathin sections were contrasted with uranyl acetate and lead citrate and analyzed using a FEI Tecnai 12 electron microscope. A peer researcher renamed the images in order to guarantee blinded quantifications by the assessor. Axonal diameters and myelin sheaths thicknesses were measured for at least 400 axons per genotype using ImageJ and G-ratios, defined as axon diameter/total axon + myelin diameter, were calculated. As most axons are not completely circular, the shortest diameter was measured. In addition, percentages of unmyelinated axons and total number of axons were quantified for at least 10 fields of view per genotype.

Histochemistry and immunohistochemistry

From our collection of VWM patient brain tissue, tissue of 14 patients, involving seven different brain regions (frontal, temporal, parietal, and occipital lobes; corpus callosum; internal capsule; and cerebellum) was analyzed by two different investigators. However, being archive material, only qualitative microscopic analysis of previously stained sections was possible and no additional stains for quantification could be performed. Formalin-fixed, paraffin-embedded tissue sections (6 μm thick) were deparaffinized and stained with haematoxylin and eosin or Bodian. For immunohistochemistry, heat-induced antigen retrieval was performed in 0.01 mol/L citrate buffer (pH 6) in microwave at low setting, followed by incubation with antibodies against NF (MON3004; 1:50; Monosan), MBP (MAB387; 1:50; EMD Millipore), proteolipid protein (MCA839G; 1:3,000; AbD Serotec), phosphorylated neurofilament (SMI-31R, 1:1000, Covance), or non-phosphorylated neurofilament (SMI-32R, 1:1000, Covance) and subsequently a horseradish peroxidase secondary antibody. Immunopositivity was detected with 3,3'-Diaminobenzidine (DAB) as chromogen. Images were acquired on a Leica DM6000B microscope (Leica Microsystems).

Golgi staining procedure

Golgi stain was performed on fresh 4-month-old mouse brains (two wild-type and two *2b5^{ho}* mice) using the FD

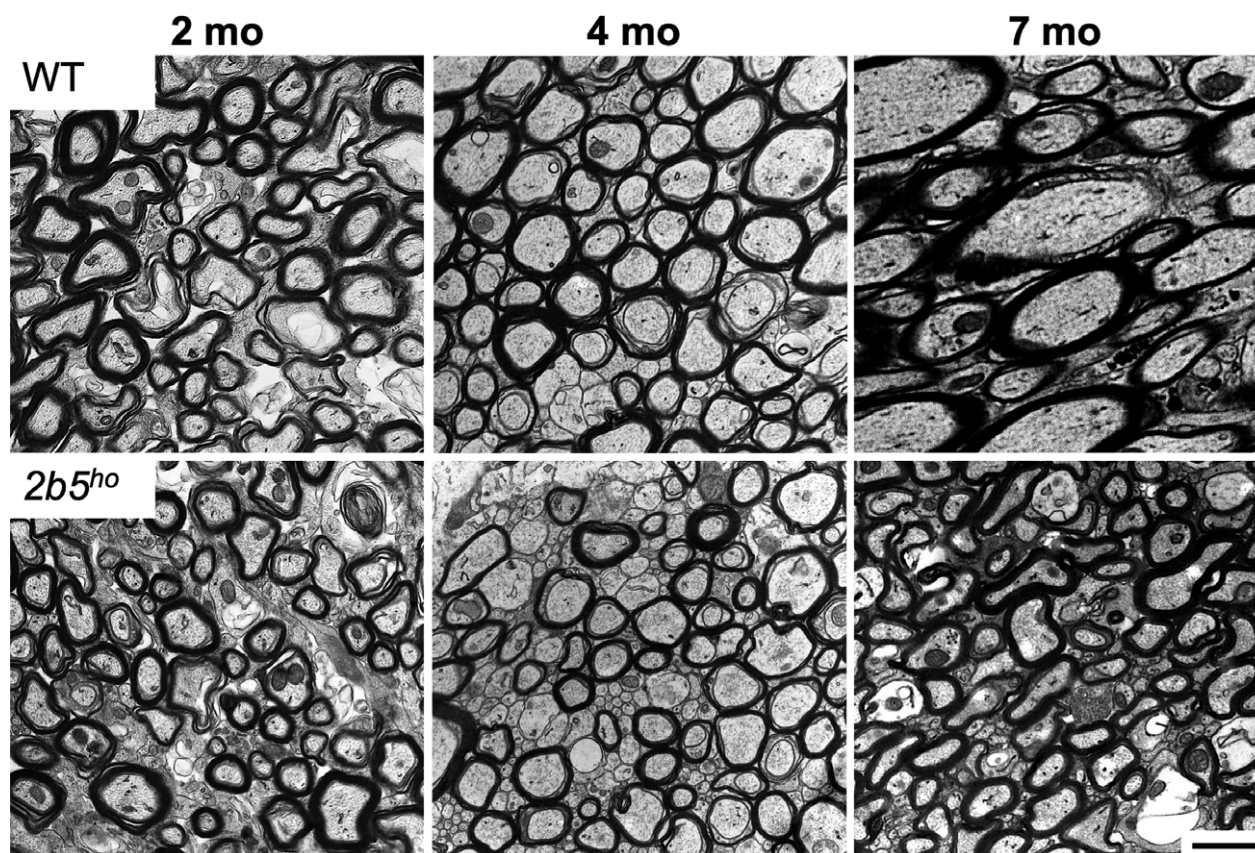


Figure 1. EM pictures of wild-type and $2b5^{ho}$ mouse corpus callosum at 2, 4, and 7 months of age. Axonal diameters in 7-month-old $2b5^{ho}$ are smaller than in wild-type mice. Scale bar: 1 μm for all pictures.

Rapid GolgiStain Kit (FD Neurotechnologies, Inc.) according to the manufacturer's instructions. Tissue sections were cut at 150 μm , stained, and coverslipped with DePeX (Serva), after which images were acquired on a confocal microscope (Zeiss LSM510) with a 10x objective (numerical aperture 0.3, 0.7x mechanical zoom) or a 40x oil objective (numerical aperture 1.3, 1x or 2.5x mechanical zoom), as z stacks with a 1- μm interval. Images were analyzed with the freely available RECONSTRUCT software (<http://synapses.clm.utexas.edu>).³² Spine densities were determined along primary apical dendrites of layer V pyramidal neurons, starting quantification at a distance of 25 μm from the cell body.

Statistical analysis

Mouse EM data were tested for median differences using Mann–Whitney U test or Kruskal–Wallis test followed by post hoc Mann–Whitney U test, as assumptions for parametric tests were not met.

Independent co-culture experiments were performed at least four times with at least three replicates per

co-culture condition. To analyze the data of all experiments simultaneously, we ran a multi-level analysis with experiment as clustering variable. Astrocyte genotype, forebrain genotype, and their interaction term were included as fixed effects. The interaction term between astrocyte and forebrain mixed cells was removed from the models in case this term was not significant. To accommodate variation across experiments in a specific outcome parameter, and variation in the effects of astrocyte genotype and forebrain genotype, random effects for these parameters were included in the model as nuisance parameters. Data are presented in multiple plots comparing two possible combinations of astrocyte-forebrain (wild-type vs. $2b5^{ho}$ cells) co-cultures, with each data point representing the mean of an individually performed experiment. Spine data were analyzed using an independent Student's *t* test.

All data were analyzed using two-sided tests. As effect size, Pearson's correlation coefficient *r* was used, with values of .10, .30, and .50 denoting a small, medium or large effect, respectively. A Bonferroni correction of the α was applied (standard $\alpha = 0.05$) when performing multiple

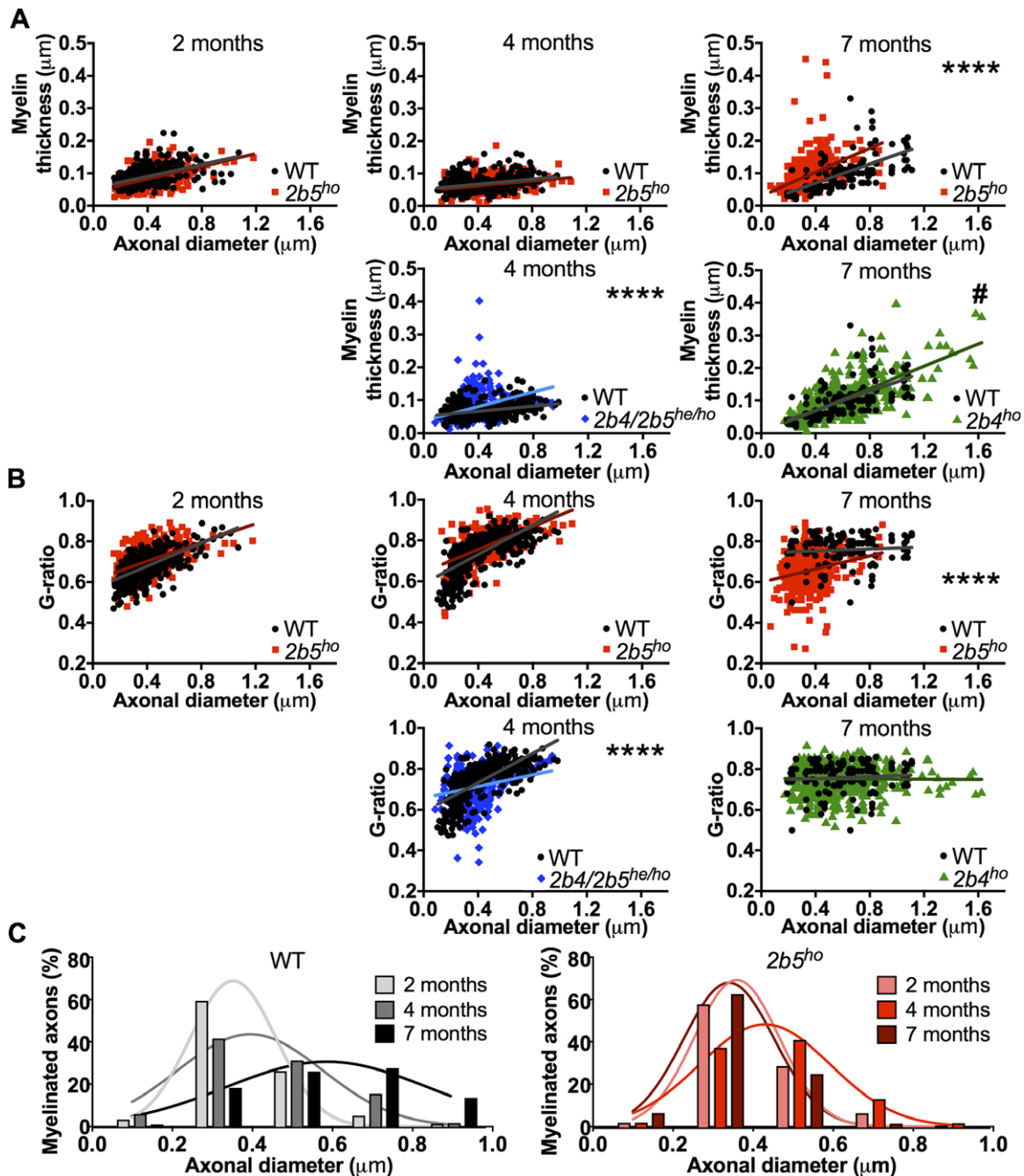


Figure 2. Disproportionally smaller axonal diameter and lower G-ratio in VWM mouse corpus callosum in more severely affected animals. (A) Whereas axonal diameter and myelin sheath thickness were normal or close to normal in 2- and 4-month-old *2b5^{ho}* mice, axonal diameter was smaller in 7-month-old *2b5^{ho}* than in wild-type mice (wild-type median 0.61 vs. *2b5^{ho}* median 0.33, $Z = -11.05$, $****P < 0.0001$, $r = 0.46$), while myelin sheath thickness remained close to normal. In the *2b4/2b5^{heho}* mice, myelin sheaths were thicker than normal (wild-type median 0.64 vs. *2b4/2b5^{heho}* median 0.75, $Z = -3.91$, $****P < 0.0001$, $r = 0.14$). In the *2b4^{ho}* mice, the axons were smaller compared to wild-type mice (wild-type median 0.61 vs. *2b4^{ho}* median 0.49, $Z = -2.89$, $\#P = 0.0039$, $r = 0.11$; which is a borderline significant trend with a Bonferroni-corrected P value of 0.0033 for all 15 comparisons performed in **A** and **B**). Slopes of correlations between myelin sheath thickness and axonal diameter were similar between wild-type mice and *2b4^{ho}* and *2b5^{ho}* mutants, but slightly higher in the 4-month-old *2b4/2b5^{heho}* mice. (B) G-ratio's were comparable in 2- and 4-month-old wild-type and *2b5^{ho}* mice and in 7-month-old wild-type and *2b4^{ho}* mice. Aberrant G-ratios were detected for 4-month-old *2b4/2b5^{heho}* mice (wild-type median 0.76 vs. *2b4/2b5^{heho}* median 0.72, $Z = -5.78$, $****P < 0.0001$, $r = 0.20$) and 7-month-old *2b5^{ho}* mice (wild-type median 0.78 vs. *2b5^{ho}* median 0.66, $Z = -11.68$, $****P < 0.001$, $r = 0.49$). (C) Wild-type mice showed a clear shift to thicker myelinated axons from 2 to 4, to 7 months of age, whereas the *2b5^{ho}* mice showed a shift to thicker axons from 2 to 4 months but shifted back to smaller axons at 7 months, comparable as the 2-month-old mice. (A, B) Mann-Whitney U test.

comparisons. Normality tests and multi-level analyses were performed using IBM SPSS Statistics 22. All other statistical analysis and plots were carried out and prepared using Prism 6.0 (GraphPad Software, Inc).

Study approval

Mouse brain tissue was obtained in strict compliance with the animal welfare policies of the Dutch government and approved by the IACUC of the VU University of Amsterdam. Written informed consent was obtained according to the Declaration of Helsinki and was provided by

patients or their parents for the collection and use of patients' samples. The Medical Ethics committee of the VU University Medical Centre approved the procedures.

Results

Secondary axonal atrophy in VWM mice

EM analysis of the corpus callosum of mice of different ages was performed to investigate the onset and development of possible abnormalities in axon size and axon-myelin proportion (Fig. 1). There was an impact of

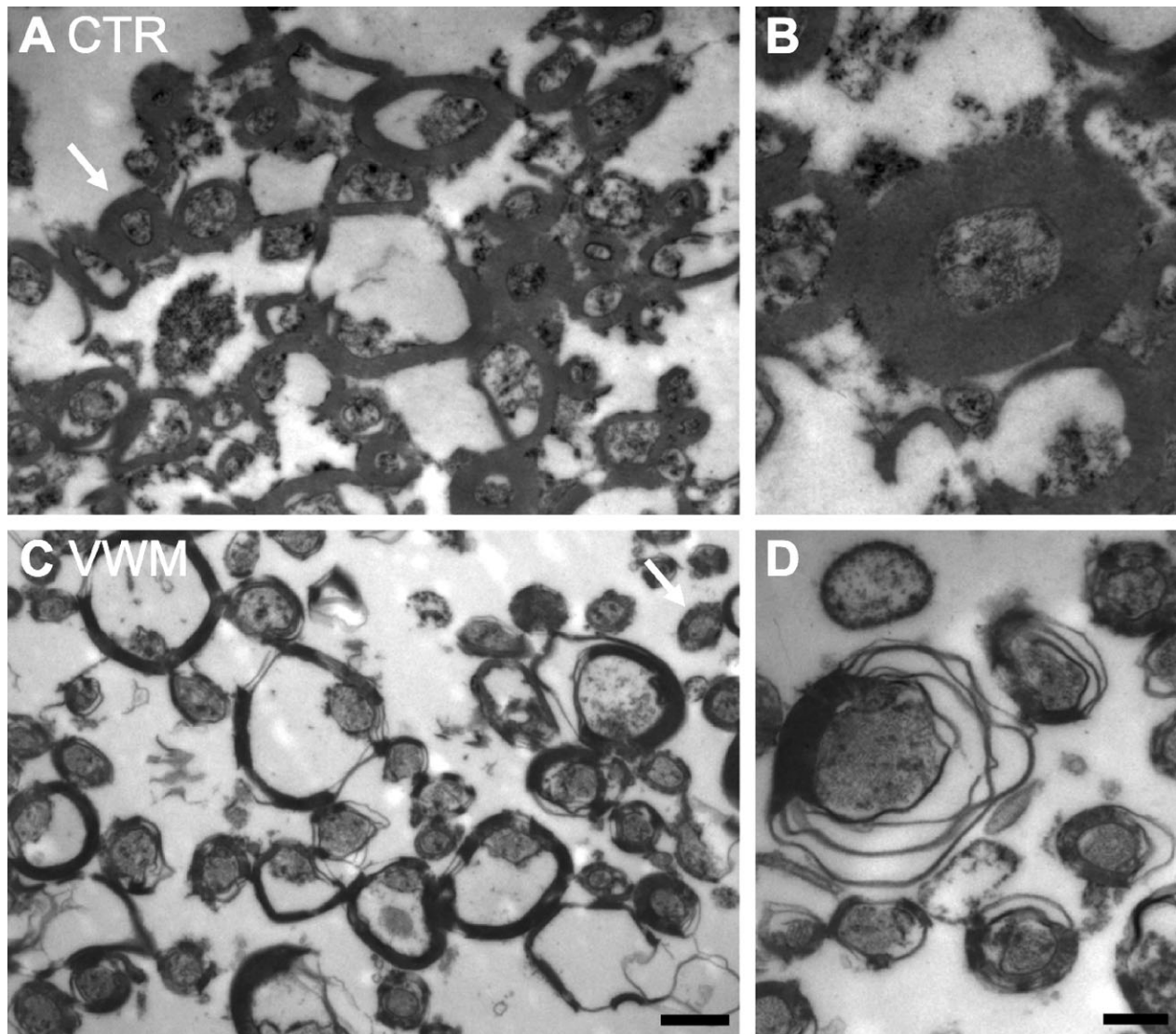


Figure 3. Thinner myelin in vanishing white matter patients' corpus callosum. EM on formalin-fixed tissue of (A, B) a control and (C, D) a vanishing white matter subject showed that, although several tissue preparation artifacts were present, myelin sheaths were thinner in patients' corpus callosum than in the control (arrows indicate axons of similar size but with different myelin sheath thicknesses). (A, C) Scale bar: 1 μ m. (B, D) Pictures zoomed in on an axon. Scale bar: 500 nm.

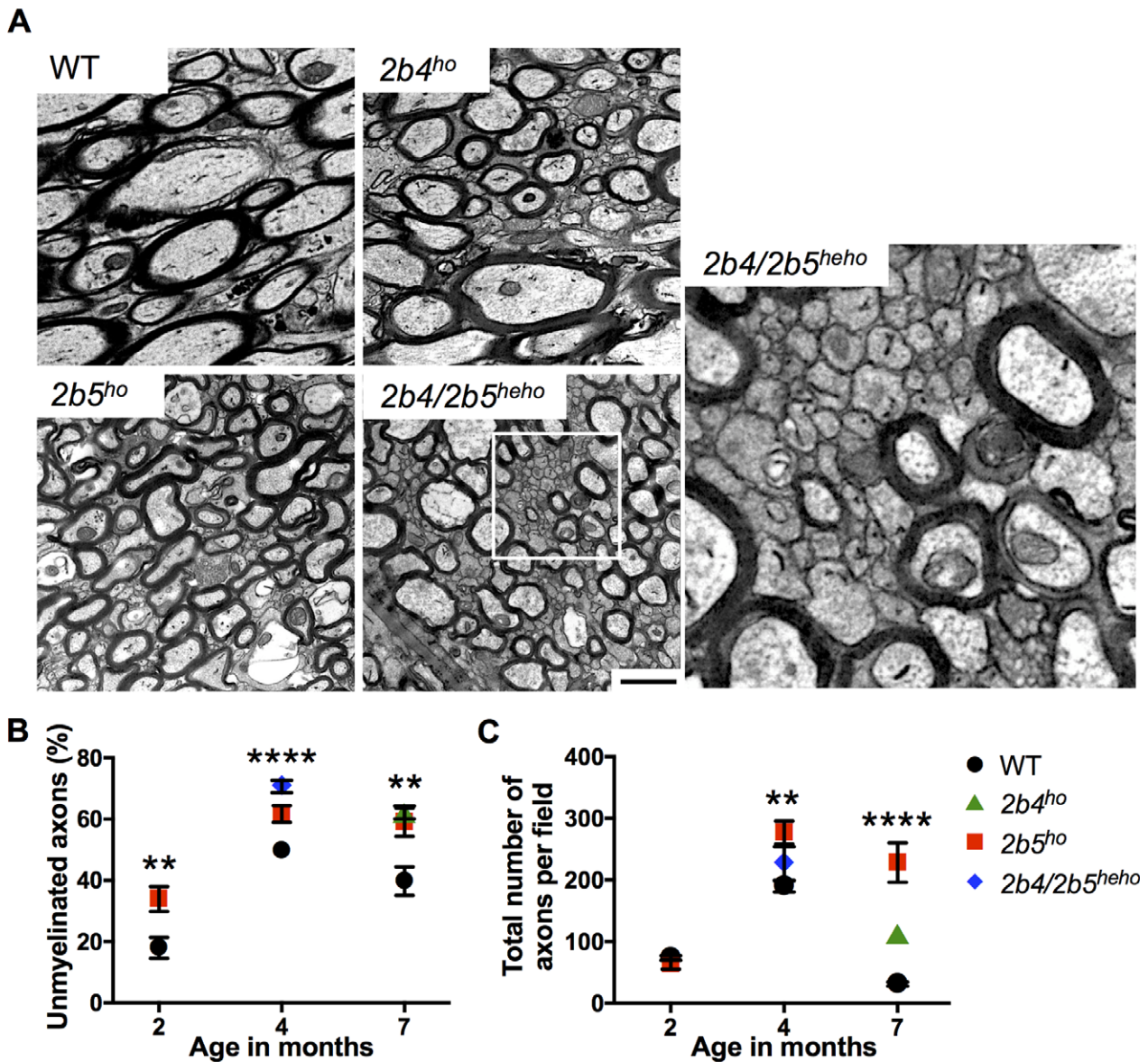


Figure 4. More thin unmyelinated axons and higher axonal density in VWM mouse corpus callosum. **(A)** EM pictures showing thin and unmyelinated axons in corpus callosum of 7-month-old *2b4^{ho}* and *2b5^{ho}* mice and 4-month-old *2b4/2b5^{heho}* mice compared to 7-month-old wild-type mice. Scale bar: 1 μm for all pictures. Picture on the right is zoomed in picture of *2b4/2b5^{heho}* mouse. **(B)** Quantification (at least 10 fields of view per genotype and age) showed higher percentages of unmyelinated axons in VWM mice than in wild-type mice at 2 months (wild-type median 11 vs. *2b5^{ho}* median 35, $Z = -2.88$, $**P < 0.01$, $r = 0.47$ by Mann–Whitney U test), 4 months ($H(2) = 22.81$, $****P < 0.0001$ by Kruskal–Wallis test, where *2b5^{ho}* and *2b4/2b5^{heho}* mice differ from wild-type mice by Mann–Whitney U test, $Z = -3.17$, $P < 0.01$, $r = 0.48$ and $Z = 4.38$, $P < 0.0001$, $r = 0.74$, respectively), and 7 months ($H(2) = 9.65$, $**P < 0.01$ by Kruskal–Wallis test, where *2b4^{ho}* and *2b5^{ho}* mice differ significantly from wild-type mice by Mann–Whitney U test, $Z = -2.80$, $P < 0.01$, $r = 0.52$ and $Z = -2.09$, P value below Bonferroni-corrected P of 0.025, $r = 0.40$, respectively). **(C)** Quantification of the total number of axons per field of view (at least 10 fields of view per genotype and age) showed higher axonal densities in the VWM mice than in the wild-type mice at 4 months ($H(2) = 12.93$, $**P < 0.01$ by Kruskal–Wallis test, where *2b5^{ho}* mice differ from wild-type mice by Mann–Whitney U test, $Z = -3.66$, $P < 0.001$, $r = 0.55$) and 7 months ($H(2) = 29.85$, $****P < 0.0001$ by Kruskal–Wallis test, where *2b4^{ho}* and *2b5^{ho}* mice differ from wild-type mice by Mann–Whitney U test, $Z = -4.32$, $P < 0.0001$, $r = 0.80$ and $Z = -4.36$, $P < 0.0001$, $r = 0.81$, respectively). Data represent mean \pm SEM.

disease severity on axon diameter and axon diameter-myelin thickness ratio. In clinically presymptomatic *2b5^{ho}* mice at 2 and 4 months, no clear differences were seen

compared to wild-type mice, although myelin sheaths tended to be slightly thinner (Fig. 2A, B). By contrast, in clinically symptomatic *2b5^{ho}* mice at 7 months, clear

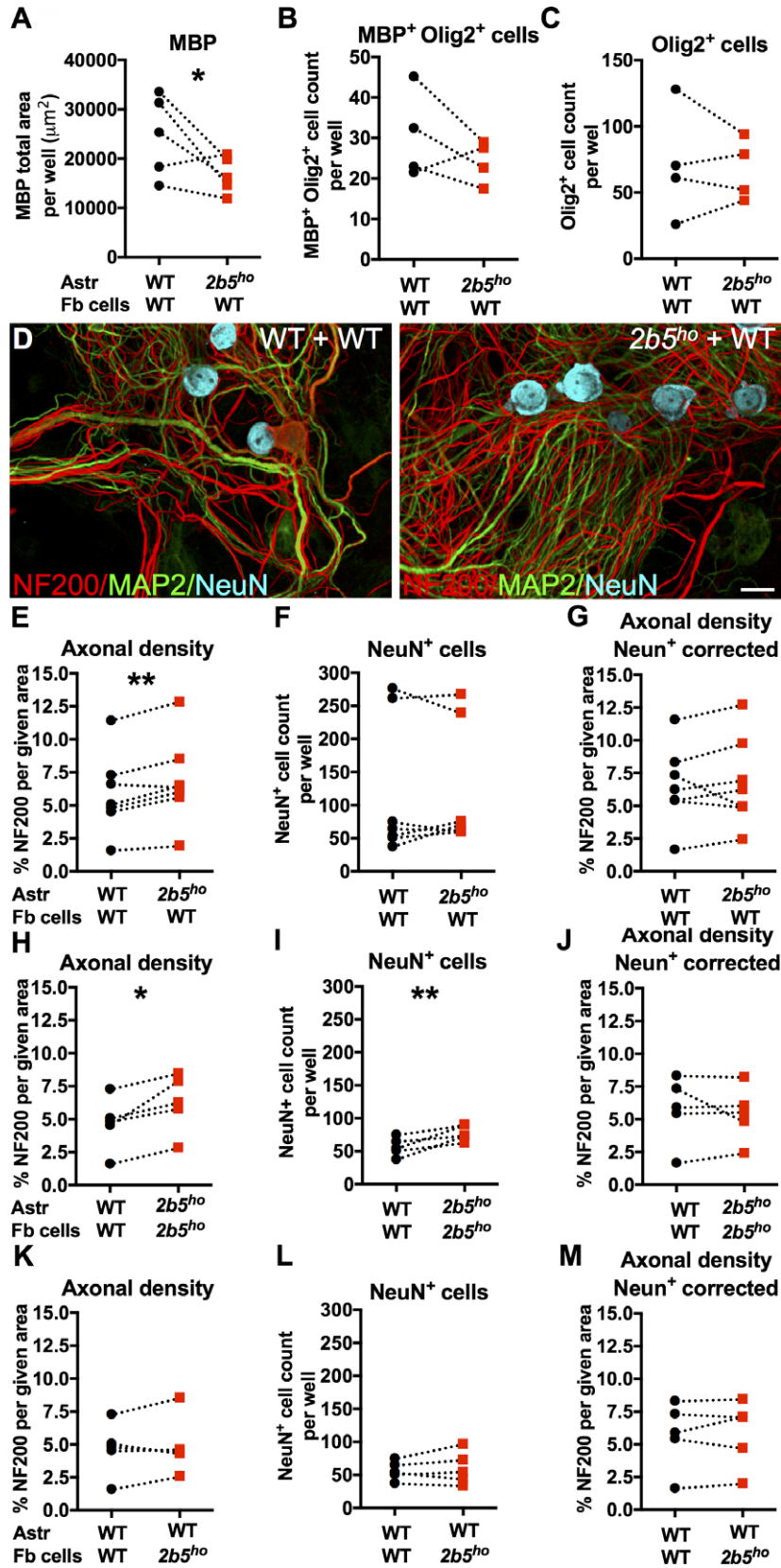


Figure 5. Higher axonal density in VWM astrocyte-based co-culture. (A) MBP amounts ($t(5.03) = -2.73$, $P < 0.05$, $r = 0.77$) and in most cultures (B) percentages of MBP-expressing Olig2⁺ cell numbers (although overall not significant, $t(4.03) = -1.69$, $P = 0.17$, $r = 0.64$) were lower when wild-type forebrain mixed cells were cultured on $2b5^{ho}$ astrocytes than if cultured on wild-type astrocytes, while having no effect on (C) the total number of Olig2⁺ cells ($P = 0.68$). (D) Co-culture of wild-type forebrain cells on wild-type versus $2b5^{ho}$ astrocytes stained for axons (NF200, red), dendrites (MAP2, green), and neuronal cell bodies (NeuN, cyan). For the sake of clarity, the astrocytes themselves are not shown. Scale bar: 20 μm . A higher axonal density was obtained when wild-type forebrain cells ($t(7.07) = 3.86$, $**P < 0.01$, $r = .82$, (E) or $2b5^{ho}$ forebrain cells ($t(5.07) = 2.52$, $P = .052$, $r = 0.75$, not shown) were cultured on $2b5^{ho}$ astrocytes than on wild-type astrocytes, which was partly related to variance in neuronal cell numbers (F, G). (H) A similar effect on axonal density was detected in cultures consisting of two layers of $2b5^{ho}$ cells in comparison to wild-type cells ($t(5.10) = 3.92$, $*P < 0.05$, $r = 0.89$), associated with a higher neuronal cell number ($t(49.08) = 3.28$, $**P < 0.01$, $r = 0.42$, (I, J). No effect on axonal density was detected when $2b5^{ho}$ forebrain cells in comparison to wild-type forebrain cells were cultured on either wild-type astrocytes (K-M) or $2b5^{ho}$ astrocytes (not shown). (E-M) The different plots present data of the same five to seven individual experiments. Each data point represents the mean of an individually performed experiment, for the specified co-culture combination. Statistics were obtained by multi-level analysis on the raw data of all experiments combined. Astr = astrocyte monolayer; Fb cells = forebrain cells.

differences were seen. While myelin sheaths remained on average slightly thinner than in wild-type mice, axons had become disproportionately thin for the myelin sheath thickness, resulting in a lower G-ratio than in wild-type mice, especially for thinner axons (Figs. 1 and 2A, B). Interestingly, a few myelin sheaths were much thicker than normal. In the more severely affected $2b4/2b5^{heho}$ mice, abnormalities were already present at 4 months, which is end-stage for these mutants. Myelin sheaths were thicker and axons were slightly thinner than in 4-month-old wild-type mice, resulting in a decreased G-ratio (Fig. 2A, B). Strikingly, again a few myelin sheaths were seen that were much thicker than normal. In the less severely affected $2b4^{ho}$ mice, abnormalities were less obvious; myelin sheaths were close to normal, but axons were relatively small, although with a striking variation in diameter and presence of several very thick axons. Like wild-type mice, the G-ratio was similar for different axonal sizes. A few myelin sheaths were thicker than normal, but less so than in 4-month-old $2b4/2b5^{heho}$ mice and 7-month-old $2b5^{ho}$ mice.

Regarding the diameter distribution of myelinated axons at different ages, an increase in axonal size in both $2b5^{ho}$ mutant and wild-type mice occurred between 2 and 4 months, with a further increase in 7-month-old wild-type mice, while axonal diameter distribution in 7-month-old $2b5^{ho}$ mice had reversed to that of 2-month-old mice, indicating secondary axonal atrophy (Fig. 2C). Regarding variation in myelin sheath thickness in wild-type and $2b5^{ho}$ mice at different ages, $2b5^{ho}$ mice had slightly higher frequencies of very thin sheaths at 2 and 4 months and a greater variation in thickness at 7 months (data not shown).

Thin myelin sheaths and axons in VWM patients

EM analysis of human corpus callosum clearly showed thinner myelin sheaths in the VWM patient than in the control, but because of postmortem artifacts and long-

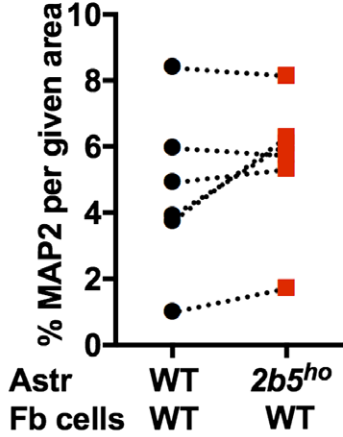
term storage in formalin before being processed for EM, no reliable quantification and statistical analysis could be performed (Fig. 3). Histochemical and immunohistochemical analysis of patients brain tissue revealed that axons were normal where tissue damage was mild (mild tissue rarefaction), but were thin where tissue damage was at least moderate (severe tissue rarefaction to cavitation, data not shown).

High numbers of thin, unmyelinated axons and increased axonal density in $2b5^{ho}$ mouse corpus callosum; increased axonal density in primary co-cultures

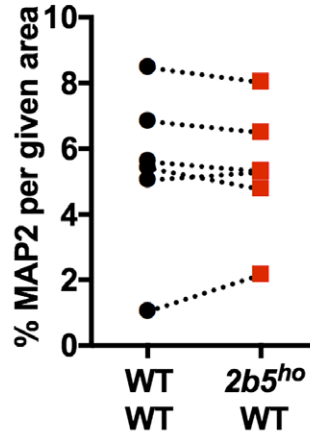
EM analyses of 7-month-old wild-type, $2b4^{ho}$, $2b5^{ho}$ and 4-month-old $2b4/2b5^{heho}$ mice revealed presence of many thin, unmyelinated axons in the mutants' corpus callosum, with the highest numbers in the double-mutants (Fig. 4A). Additional EM analyses of younger animals showed that higher percentages of thin unmyelinated axons were already present from 2 months onward, although less high than at 4 and 7 months (Fig. 4B). These thin axons were associated with a higher axonal density at 4 and 7 months (Fig. 4C).

In order to further explore the development of axonal abnormalities, we prepared primary myelinating cell cultures consisting of a layer of mouse forebrain mixed cells, including neurons, oligodendrocytes, microglia, and a few astrocytes, plated on a monolayer of mouse forebrain-derived astrocytes, cultured together for 4 weeks. The astrocyte monolayers contained ~6.5% or ~3.1% microglia when derived from wild-type or $2b5^{ho}$ mice, respectively (data not shown). Co-culture data of all experiments were analyzed simultaneously with multi-level analysis. When cultured with wild-type mixed forebrain cells, a monolayer of $2b5^{ho}$ astrocytes suppressed total MBP amounts compared to a monolayer of wild-type astrocytes, (Fig. 5A, $t(5.03) = -2.73$, $P < 0.05$, $r = 0.77$) and in most cultures, the percentage of Olig2-positive cells expressing MBP, although the latter was

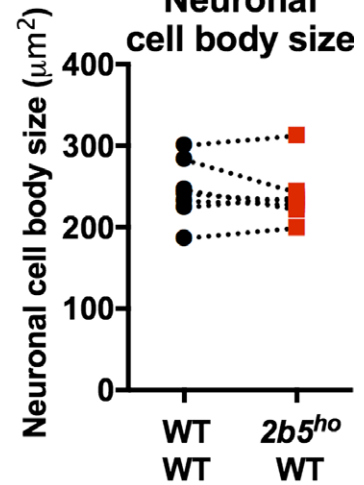
A Dendritic density



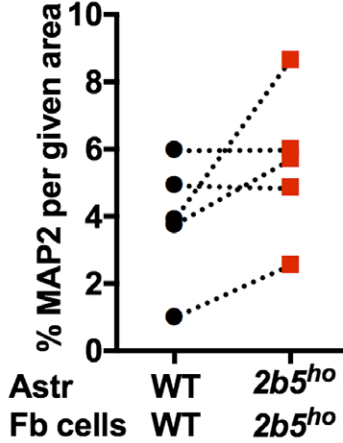
B Dendritic density
Neun⁺ corrected



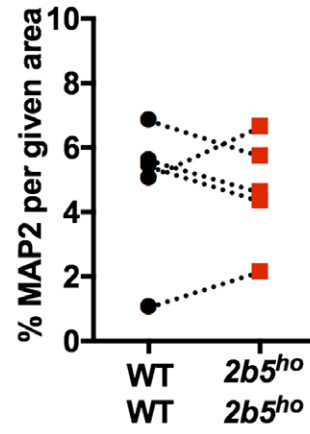
C Neuronal cell body size



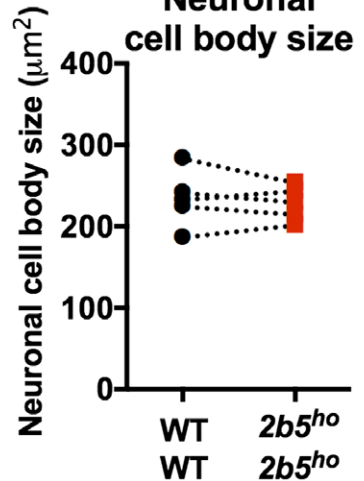
D Dendritic density



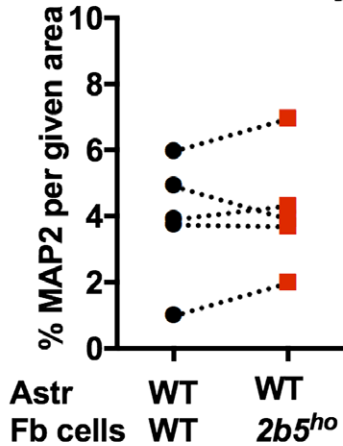
E Dendritic density
Neun⁺ corrected



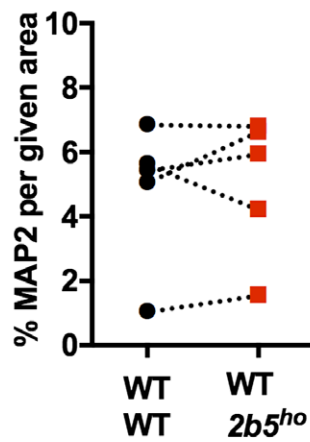
F Neuronal cell body size



G Dendritic density



H Dendritic density
Neun⁺ corrected



I Neuronal cell body size

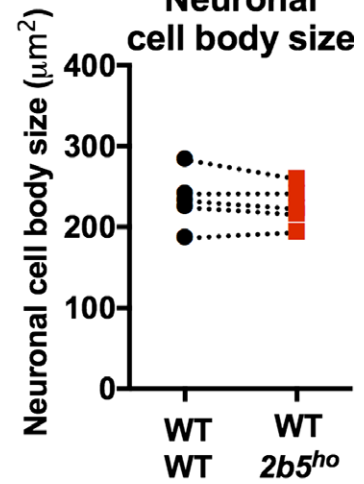


Figure 6. No significant differences in dendritic density and neuronal cell body size between co-cultures consisting of $2b5^{ho}$ versus wild-type mouse-derived cells. No effect of $2b5^{ho}$ in comparison to wild-type astrocytes on neuronal cell body size was detected when wild-type forebrain cells (A-C) or $2b5^{ho}$ forebrain cells (not shown) were cultured on top. Also two layers of $2b5^{ho}$ versus wild-type cells (D-F) or $2b5^{ho}$ forebrain cells on either (C) wild-type astrocytes or $2b5^{ho}$ astrocytes (not shown) did not give a difference in dendritic density or neuronal cell body size. (A-I) The different plots present data of the same five to seven individual experiments, the same experiments as plotted in Fig. 4. Each data point represents the mean of an individually performed experiment, for the specified co-culture combination. Statistics were obtained by multi-level analysis on the raw data of all experiments combined. Astr = astrocyte monolayer; Fb cells = forebrain cells.

overall not significant (Fig. 5B, $t(4.03) = -1.69$, $P = 0.17$, $r = 0.64$), while having no effect on the total number of Olig2⁺ cells (Fig. 5C, $P = 0.68$).

Regarding the effect of $2b5^{ho}$ astrocytes compared to wild-type astrocytes on axonal density, we found a significant main fixed effect for astrocyte ($t(6.88) = 3.48$, $P < .01$, $r = 0.80$), but no main fixed effect for forebrain mixed cells ($t(4.92) = 1.31$, ns, $r = 0.51$), indicating that the genotype of the astrocyte monolayer does affect axonal density, but the genotype of the forebrain mixed cells on top does not. Further analysis demonstrated that the $2b5^{ho}$ astrocyte monolayers promoted a higher axonal density than wild-type astrocyte monolayers in wild-type forebrain cells (Fig. 5D, E; $t(7.07) = 3.86$, $P < 0.01$, $r = 0.82$) without changing neuronal cell numbers (Fig. 5F, G). The difference in the effect of $2b5^{ho}$ astrocytes compared to wild-type astrocytes on axonal density for $2b5^{ho}$ forebrain cells was smaller (data not shown; borderline significance, $t(5.07) = 2.52$, $P = .052$, $r = 0.75$). Comparing cultures in which both the astrocyte and forebrain layers were either $2b5^{ho}$ mutant or wild-type showed that the effect of mutant astrocytes compared to wild-type astrocytes on axonal density was similar to the effects observed in wild-type forebrain cells (Fig. 5H; $t(5.10) = 3.92$, $P = 0.01$, $r = 0.89$, vs. Fig. 5E), indicating lack of a significant additional effect of the mutant forebrain cells on axonal density. Neuronal cell numbers in cultures with both layers consisting of $2b5^{ho}$ cells were higher than when both layers consisting of wild-type cells ($t(49.08) = 3.28$, $P < 0.01$, $r = 0.42$, Fig. 5I, J), indicating some effect of the mutant astrocytes combined with the

mutant forebrain cells on neuronal cell number. When cultured on wild-type astrocytes, $2b5^{ho}$ forebrain cells had no effects on axonal density or neuronal cell number compared to wild-type forebrain cells (Fig. 5K–M) and neither did they have an effect when cultured on $2b5^{ho}$ astrocytes (data not shown).

Regarding effects on dendritic density, neuronal cell body size and on the ratio between axonal and dendritic density, no significant differences were detected with these combinations of wild-type or $2b5^{ho}$ astrocytes and forebrain cells (Fig. 6 and data not shown).

Evidence of mild axonal damage in VWM patient white matter

In order to assess whether axonal swellings and spheroids primarily occur in regions with severe tissue damage, we microscopically examined brain tissue of VWM patients for the presence of axonal swellings and spheroids using immunohistochemistry. In most patients, only a few scattered swellings and spheroids were detected (Fig. 7A). Also in severely damaged tissue only a few spheroids were found (Fig. 7B), the presence of which was not dependent on brain region (Fig. 7C). Of note was the presence of many spheroids in the occipital lobe of one of the oldest VWM patients (37 years at demise, Fig. 7D), while tissue structure and myelin content (not shown) were relatively preserved. No obvious signs of impaired axonal cytoskeletal architecture (SMI31 vs. SMI32) were detected in patient tissue and co-culture experiments (data not shown).

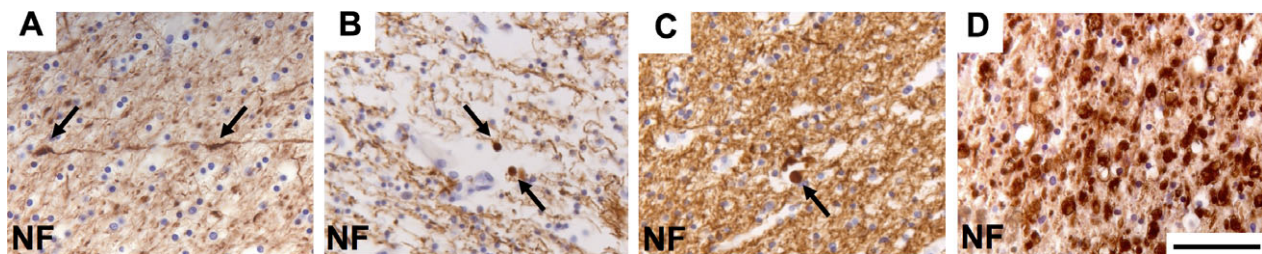


Figure 7. Axonal damage in VWM patients' white matter. (A) NF-staining of frontal lobe of a 37-yr-old VWM patient showed a few swellings (arrows). (B) Frontal lobe of a 10-yr-old VWM patient showed a few spheroids (arrows), whereas tissue damage was severe. (C) Internal capsule of the same 10-yr-old VWM patient showed one spheroid (arrow), whereas tissue damage was meager. (D) NF staining of occipital lobe of the same 37-yr-old VWM patient showed many axonal swellings and spheroids, while the tissue and myelin (not shown) was relatively intact. Scale bar: 50 μ m for all.

Unaffected synapse or spine density in primary co-cultures or along primary apical dendrites of layer V pyramidal neurons

Synaptic densities were quantified in co-cultures of various combinations of wild-type and *2b5^{ho}* mouse-derived cells (Fig. 8A–F). No difference in synaptic density was found when wild-type forebrain mixed cells ($P = 0.17$, Fig. 8D) or *2b5^{ho}* forebrain mixed cells ($P = 0.40$, not shown) were cultured on a monolayer of *2b5^{ho}* astrocytes compared to wild-type astrocytes. Also no significant effect of *2b5^{ho}* versus wild-type forebrain cells on synaptic density was found with either wild-type astrocytes ($P = 0.09$, Fig. 8E) or *2b5^{ho}* astrocytes ($P = 0.20$, data not shown). A trend for a lower synaptic density was found when both layers consisted of *2b5^{ho}* cells compared to two layers of wild-type cells ($t(5.09) = -2.334$, $P = 0.07$, $r = 0.72$; Fig. 8F).

In Golgi stains of fresh 4-month-old mouse brains (Fig. 8G–I), no difference in spine density was detected along apical dendrites of wild-type versus *2b5^{ho}* layer V pyramidal neurons (Fig. 8I).

Discussion

VWM is a devastating leukodystrophy, for which the underlying cellular mechanisms have yet to be unraveled. The current view is that astrocytes and oligodendrocytes are selectively affected, and that astrocyte pathology drives oligodendrocyte pathology.²³ We previously developed mutant VWM mice that are representative of the human disease.²³ Here, we studied axonal abnormalities in VWM *Eif2b4*- and *Eif2b5*- mutant mice with different disease severities and of different ages, in order to assess whether and when axonal abnormalities occur. In addition, we used primary astrocyte-forebrain co-cultures based on brain cells of the *Eif2b5* mice to assess whether axonal abnormalities are primary or secondary to abnormality of VWM astrocytes. We verified findings in brain tissue of patients.

In *2b5^{ho}* mice, average axonal diameter and relative myelin sheath thickness and their variation are initially normal, although myelin sheaths tend to be slightly thinner from early on. It is only at 7 months that axons are disproportionately small and myelin sheaths are still slightly thinner than normal, but thicker than expected for the axonal diameter, reflected by a lower G-ratio, especially for the smaller axonal diameters. The distribution of axonal diameters in *2b5^{ho}* mice is close to normal at 2 and 4 months with a normal shift to greater axonal diameters at 4 months. However, the distribution of axonal diameters at 7 months has returned to that at 2 months, while in wild-type mice, a further shift to larger diameters has occurred. In the more severely affected

2b4/2b5^{heho} mice, deviating results for axonal diameter, relative myelin sheath thickness, and G-ratio are already present at 4 months. In the less severely affected *2b4^{ho}* mice, differences from wild-type mice at the age of 7 months are less clear than in *2b5^{ho}* mice of the same age. Overall, our results indicate that axons and relative myelin sheath thickness are initially normal or close to normal and only secondarily axonal atrophy occurs, dependent on disease severity. Previously, a different *Eif2b5* mutant mouse model was reported to display a higher proportion of thin axons in the internal capsule associated with thinner myelin sheaths and a normal G-ratio at 3 weeks.³³ Axonal diameter and myelin sheath thickness at later ages were not reported, but it was demonstrated that in the cerebral peduncle of 15-month-old mutants an increased proportion of axons had no or thinner myelin than of wild-type mice.

The mouse findings were in part confirmed in VWM patient tissue. Notably, patient tissue was obtained at autopsy and therefore at end-stage disease, whereas mice were sacrificed at the time of appearance of clinical symptoms. EM analysis of the corpus callosum of a VWM patient suggested that myelin sheaths are thinner than in an age-matched control subject, but, as explained above, no definitive quantification of myelin sheath thickness or axonal diameter could be performed. However, examination of multiple patients' white matter regions overall demonstrated that axons were normal where tissue damage was mild, but were thin where tissue damage was moderate to severe, in line with the findings in the VWM mice. Thin axons in human brain tissue have been described before.⁶ Taken together, these data indicate that axonal morphological aberrancies are related to the severity of the white matter disease.

A new finding is the presence of numerous thin, unmyelinated axons in the corpus callosum of mutant mice, not present in similar numbers in wild-type mice, resulting in increased axonal density. The highest percentage was found in the most severely affected *2b4/2b5^{heho}* mice, suggesting that the density of thin unmyelinated axons also correlates with disease severity. Our mouse astrocyte-forebrain co-culture model provided us with the opportunity to assess if axonal density is related to the influence of mutant astrocytes on axons. Interestingly, in *2b5^{ho}* mouse-derived cell cultures axonal density is also increased compared to wild-type cultures. A layer of *2b5^{ho}* astrocytes suffices to achieve this effect in wild-type or *2b5^{ho}* forebrain cells; a layer of *2b5^{ho}* astrocytes cultured with *2b5^{ho}* forebrain cells does not have an additional effect. Notably, a layer of *2b5^{ho}* forebrain cells on wild-type astrocytes is associated with a normal axonal density. These findings indicate that the effect is not intrinsic to axons or neurons, but mediated by *2b5^{ho}*

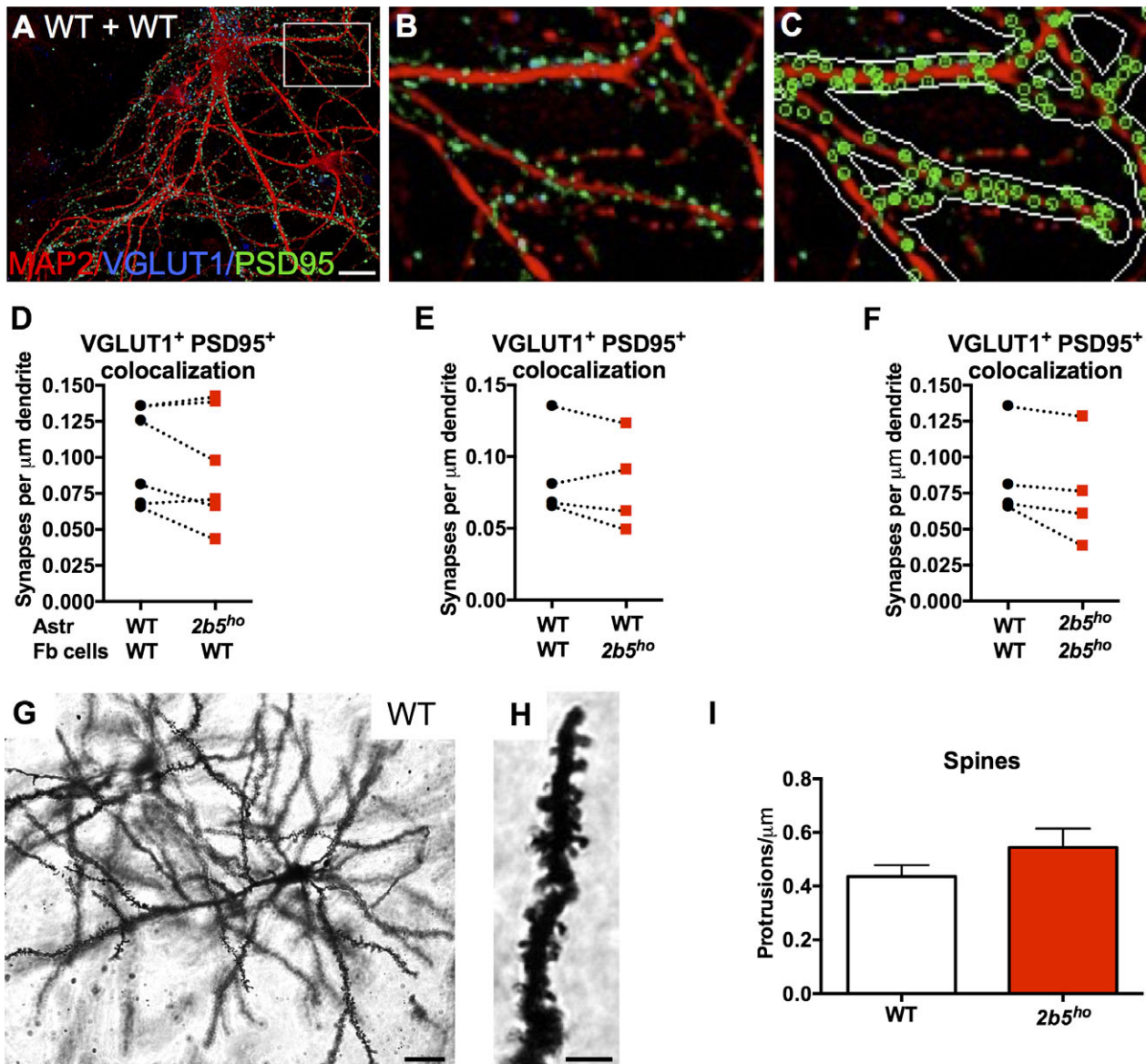


Figure 8. No difference in synapse or spine density in primary co-cultures or along primary apical dendrites of layer V pyramidal neurons (A) Co-culture of wild-type forebrain cells on wild-type astrocytes stained for dendrites (MAP2, red), presynapses (VGLUT1, cyan), and postsynapses (PSD95, green). For the sake of clarity, the astrocytes themselves are not shown. Scale bar: 20 μm . (B) Zoomed in picture of boxed area in A. (C) Identification of dendrites and synapses included in quantification. No difference in synaptic density was detected when wild-type forebrain cells (D) or *2b5^{ho}* forebrain cells (not shown) were cultured on *2b5^{ho}* astrocytes compared to wild-type astrocytes ($P = 0.17$ and $P = 0.40$, respectively). Also no significant effect of *2b5^{ho}* versus wild-type forebrain cells was detected on either (E) wild-type or (not shown) *2b5^{ho}* astrocytes ($P = 0.09$ and $P = 0.20$, respectively). (F) Two layers of *2b5^{ho}* cells in comparison to wild-type cells resulted in a trend for a lower synaptic density ($t(5.09) = -2.334$, $P = 0.07$, $r = 0.72$). (G, H) Golgi-stained mouse layer V pyramidal neuron. (G) Scale bar: 20 μm . (H) Scale bar: 5 μm . (I) No difference in spine density was detected along primary apical dendrites of wild-type and *2b5^{ho}* layer V pyramidal neurons. (D-F) The different plots present data of the same four to six individual experiments. Each data point represents the mean of an individually performed experiment, for the specified co-culture combination. Statistics were obtained by multi-level analysis on the raw data of all experiments combined. Astr = astrocyte monolayer; Fb cells = forebrain cells.

astrocytes, which promote higher axonal density. These data imply that axons are not primarily affected in VWM, but atrophy secondarily due to astrocytes or astrocyte-secreted factors.

Another new finding is the observation of some very large axons in the 7-month-old *2b4^{ho}* mice and some very thick myelin sheaths in the 4-month-old *2b4/2b5^{heho}* mice and 7-month-old *2b4^{ho}* and *2b5^{ho}* mice, associated with a

very low G-ratio. Apparently the strict relationship between axon diameter and myelin sheath thickness is disrupted in more than one way. The cause of this remains unclear.

Previously, we showed that astrocyte pathology is a first sign of the disease in VWM mice and occurs before myelin pathology: we observed immaturity of astrocytes at postnatal day 14, followed by lower than normal MBP expression at day 21 in the same *2b5^{ho}* mouse model.²³ In co-cultures of different composition, we demonstrated that oligodendrocyte maturation defect and lack of MBP production are induced by VWM astrocytes and not intrinsic to VWM oligodendrocytes.²³ In this study, we confirmed that a layer of *2b5^{ho}* astrocytes in astrocyte-forebrain co-cultures inhibits total MBP production and the percentage of MBP-expressing Olig2⁺ cells.

All available evidence indicates that VWM astrocytes are primarily affected and axonal pathology is also secondary. It is an open question whether the process of axonal dystrophy is directly caused by the astrocytes through, for example, lack of energy supply or secretion of a toxic factor, or mediated through the impact of astrocytes on oligodendrocytes and their ability to provide metabolic support to axons.^{34,35} The effect of astrocytes on axonal density may be related to immaturity of VWM astrocytes, which better promote axonal growth or regeneration than mature astrocytes, while having no differential effect on dendrite growth.^{36–39} It has been postulated that astrocytes provide general support for process growth through secreted factors and that the differential effect of mature versus immature astrocytes on axonal growth, but not on dendritic growth, is due to cell-cell contact.⁴⁰

Axonal swellings and spheroids, evidence of disturbed axonal transport, are rare in VWM patient tissue. Most patients have only a few scattered swellings or spheroids throughout the brain white matter, even in the presence of severe white matter damage. The current observation of the highest number of spheroids in one of our oldest patients, and the previous observation of spheroids in older but not in younger *2b5^{ho}* mice suggests that axonal transport problems develop over time.²³ The mechanism is unclear. We found no clear signs of impaired axonal cytoskeletal architecture in patient tissue and co-culture experiments. The older patient, who had a high number of spheroids, also had relatively intact myelin, indicating that spheroids are not caused by absence of myelin. Anyhow, disturbed axonal transport does not appear to be a central problem in VWM.

It is likely that the clinical features in VWM are at least in part caused by axonal dysfunction. In our *2b5^{ho}* mice, clinical signs arise around the age of 5 months. Interestingly, the shift from normal-sized axons to disproportionately thin axons occurs between the ages of 4 and 7 months. These abnormalities potentially lead to a

reduction in signal conduction velocity, as observed in VWM patients, which correlates more closely to axon diameter than fiber (axon + myelin) diameter.⁴¹

To conclude, current data support the concept that astrocytic dysfunction drives VWM pathology, affecting not only oligodendrocyte mature functions but also the trophic condition of axons. A very important finding is that axons and relative myelin sheath thickness are initially normal or close to normal, indicating a window of opportunity for treatment. It may be possible to prevent axonal morphological changes when interventions are undertaken in time.

Acknowledgments

The authors thank the patients, families, and referring physicians for their co-operation and contribution. This work was supported by a grant from the Zeldzame Ziekten Fonds, The Netherlands. SvdS is funded by the Netherlands Scientific Organization (NWO/MaGW: VIDI-452-12-014). VMH is supported by ZonMw VIDI research grant 91712343 and E-Rare Joint Call project 9003037601. MSvdK is supported by the NWO Spinoza grant.

Author Contribution

M.D.K., M.B., and M.S.v.d.K. conceptualized and designed the study. All authors contributed to data acquisition and analysis. M.D.K. and M.S.v.d.K. primarily drafted the text; M.D.K. prepared the figures.

Conflict of Interest

Nothing to report.

References

1. van der Knaap MS, Pronk JC, Scheper GC. Vanishing white matter disease. *Lancet Neurol* 2006;5:413–423.
2. Fogli A, Schiffmann R, Bertini E, et al. The effect of genotype on the natural history of eIF2B-related leukodystrophies. *Neurology* 2004;62:1509–1517.
3. Hanefeld F, Holzbach U, Kruse B, et al. Diffuse white matter disease in three children: an encephalopathy with unique features on magnetic resonance imaging and proton magnetic resonance spectroscopy. *Neuropediatrics* 1993;24:244–248.
4. Schiffmann R, Moller JR, Trapp BD, et al. Childhood ataxia with diffuse central nervous system hypomyelination. *Ann Neurol* 1994;35:331–340.
5. van der Knaap MS, Barth PG, Gabreëls FJ, et al. A new leukoencephalopathy with vanishing white matter. *Neurology* 1997;48:845–855.

6. van der Knaap MS, Kamphorst W, Barth PG, et al. Phenotypic variation in leukoencephalopathy with vanishing white matter. *Neurology* 1998;51:540–547.
7. Leegwater PA, Vermeulen G, Könst AA, et al. Subunits of the translation initiation factor eIF2B are mutant in leukoencephalopathy with vanishing white matter. *Nat Genet* 2001;29:383–388.
8. van der Knaap MS, Leegwater PA, Könst AA, et al. Mutations in each of the five subunits of translation initiation factor eIF2B can cause leukoencephalopathy with vanishing white matter. *Ann Neurol* 2002;51:264–270.
9. Price N, Proud C. The guanine nucleotide-exchange factor, eIF-2B. *Biochimie* 1994;76:748–760.
10. van der Knaap MS, van Berkel CG, Herms J, et al. eIF2B-related disorders: antenatal onset and involvement of multiple organs. *Am J Hum Genet* 2003;73:1199–1207.
11. Bugiani M, Boor I, Powers JM, et al. Leukoencephalopathy with vanishing white matter: a review. *J Neuropathol Exp Neurol* 2010;69:987–996.
12. Brück W, Herms J, Brockmann K, et al. Myelinopathia centralis diffusa (vanishing white matter disease): evidence of apoptotic oligodendrocyte degeneration in early lesion development. *Ann Neurol* 2001;50:532–536.
13. Rodriguez D, Gelot A, Della Gaspera B, et al. Increased density of oligodendrocytes in childhood ataxia with diffuse central hypomyelination (CACH) syndrome: neuropathological and biochemical study of two cases. *Acta Neuropathol* 1999;97:469–480.
14. Bugiani M, Boor I, van Kollenburg B, et al. Defective glial maturation in vanishing white matter disease. *J Neuropathol Exp Neurol* 2011;70:69–82.
15. Dietrich J, Lacagnina M, Gass D, et al. EIF2B5 mutations compromise GFAP+ astrocyte generation in vanishing white matter leukodystrophy. *Nat Med* 2005;1:277–283.
16. van Haren K, van der Voorn JP, Peterson DR, et al. The life and death of oligodendrocytes in vanishing white matter disease. *J Neuropathol Exp Neurol* 2004;63: 618–630.
17. Bugiani M, Postma N, Polder E, et al. Hyaluronan accumulation and arrested oligodendrocyte progenitor maturation in vanishing white matter disease. *Brain* 2013;136:209–222.
18. Wong K, Armstrong RC, Gyure KA, et al. Foamy cells with oligodendroglial phenotype in childhood ataxia with diffuse central nervous system hypomyelination syndrome. *Acta Neuropathol* 2000;100:635–646.
19. Francalanci P, Eymard-Pierre E, Dionisi-Vici C, et al. Fatal infantile leukodystrophy: a severe variant of CACH/VWM syndrome, allelic to chromosome 3q27. *Neurology* 2001;57:265–270.
20. Prass K, Brück W, Schröder NW, et al. Adult-onset leukoencephalopathy with vanishing white matter presenting with dementia. *Ann Neurol* 2001;50:665–668.
21. Jansen AC, Andermann E, Niel F, et al. Leukoencephalopathy with vanishing white matter may cause progressive myoclonus epilepsy. *Epilepsia* 2008;49:910–913.
22. van der Voorn JP, van Kollenburg B, Bertrand G, et al. The unfolded protein response in vanishing white matter disease. *J Neuropathol Exp Neurol* 2005;64:770–775.
23. Dooves S, Bugiani M, Postma NL, et al. Astrocytes are central in the pathomechanisms of vanishing white matter. *J Clin Invest* 2016;126:1512–1524.
24. Nave KA, Trapp BD. Axon-glia signaling and the glial support of axon function. *Annu Rev Neurosci* 2008;31:535–561.
25. Blackburn D, Sargsyan S, Monk PN, Shaw PJ. Astrocyte function and role in motor neuron disease: a future therapeutic target? *Glia* 2009;57:1251–1264.
26. Edgar M, Nave KA. The role of CNS glia in preserving axon function. *Curr Opin Neurobiol* 2009;19:498–504.
27. McCarthy KD, de Vellis J. Preparation of separate astroglial and oligodendroglial cell cultures from rat cerebral tissue. *J Cell Biol* 1980;85:890–902.
28. Thomson CE, Hunter AM, Griffiths IR, et al. Murine spinal cord explants: a model for evaluating axonal growth and myelination in vitro. *J Neurosci Res* 2006;84: 1703–1715.
29. Sorensen A, Moffat K, Thomson C, Barnett SC. Astrocytes, but not olfactory ensheathing cells or Schwann cells, promote myelination of CNS axons in vitro. *Glia* 2008;56:750–763.
30. O'Meara RW, Ryan SD, Colognato H, Kothary R. Derivation of enriched oligodendrocyte cultures and oligodendrocyte/neuron myelinating co-cultures from post-natal murine tissues. *J Vis Exp* 2011;54:3324.
31. Pang Y, Zheng B, Kimberly SL, et al. Neuron-oligodendrocyte myelination co-culture derived from embryonic rat spinal cord and cerebral cortex. *Brain Behav* 2012;2:53–67.
32. Risher WC, Ustunkaya T, Singh Alvarado J, Eroglu C. Rapid golgi analysis method for efficient and unbiased classification of dendritic spines. *PLoS ONE* 2014;9: e107591.
33. Geva M, Cabilly Y, Assaf Y, et al. A mouse model for eukaryotic translation initiation factor 2B-leucodystrophy reveals abnormal development of brain white matter. *Brain* 2010;133:2448–2461.
34. Yin X, Crawford TO, Griffin JW, et al. Myelin-associated glycoprotein is a myelin signal that modulates the caliber of myelinated axons. *J Neurosci* 1998;18:1953–1962.
35. Nave KA, Werner HB. Myelination of the nervous system: mechanisms and functions. *Annu Rev Cell Dev Biol* 2014;30:503–533.
36. Smith GM, Rutishauser U, Silver J, Miller RH. Maturation of astrocytes in vitro alters the extent and

- molecular basis of neurite outgrowth. *Dev Biol* 1990;138:377–390.
37. Le Roux PD, Reh TA. Independent regulation of primary dendritic and axonal growth by maturing astrocytes in vitro. *Neurosci Lett* 1995;198:5–8.
38. Wunderlich G, Stichel CC, Schroeder WO, Müller HW. Transplants of immature astrocytes promote axonal regeneration in the adult rat brain. *Glia* 1994;10:49–58.
39. Filous AR, Miller JH, Coulson-Thomas YM, et al. Immature astrocytes promote CNS axonal regeneration when combined with chondroitinase ABC. *Dev Neurobiol* 2010;70:826–841.
40. Le R, Esquenazi S. Astrocytes mediate cerebral cortical neuronal axon and dendrite growth, in part, by release of fibroblast growth factor. *Neurol Res* 2002;24:81–92.
41. Gillespie MJ, Stein RB. The relationship between axon diameter, myelin thickness and conduction velocity during atrophy of mammalian peripheral nerves. *Brain Res* 1983;259:41–56.